Asian Journal of Chemistry; Vol. 24, No. 6 (2012), 2433-2441

ASIAN JOURNAL OF CHEMISTRY

www.asianjournalofchemistry.co.in

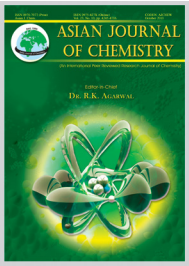

Influence of Heat Transfer and Chemical Reactions on Williamson Fluid Model for Blood Flow Through a Tapered Artery with a Stenosis

NOREEN SHER AKBAR[1,*], S. NADEEM[2,3] and CHANGHOON LEE[4]

[1]DBS&H, CEME, National University of Science and Technology, Islamabad, Pakistan
[2]Department of Mathematics, Quaid-i-Azam University, Islamabad-44000, Pakistan
[3]Department of Mathematics & Natural Sciences, Prince Mohammad Bin Fahd University, P.O. Box 1664, Al Khobar 31952, Saudi Arabia
[4]Department of Computational Sciences and Engineering, Yonsei University, Seoul, South Korea

*Corresponding author: E-mail: noreensher@yahoo.com

(*Received*: 4 April 2011; *Accepted*: 6 January 2012) AJC-10919

In the present paper, the blood flow through a tapered artery with a stenosis by considering axially non-symmetric but radially symmetric mild stenosis on blood flow characteristics is analyzed, assuming the flow is steady and blood is treated as Williamson fluid. The effects of heat and mass transfer are also carried out. Perturbation solutions have been calculated for velocity, temperature, concentration, resistance impedance, wall shear stress and shearing stress at the stenosis throat. The graphical results of different type of tapered arteries (*i.e.*, converging tapering, diverging tapering, non-tapered artery) have been examined for different parameters of interest. Stream lines have been plotted at the end of the article.

Key Words: Williamson fluid, Blood flow, Tapered artery, Stenosis, Perturbation solution, Heat and mass transfer.

INTRODUCTION

The algorithm of calculation of hypothermia and hyperthermia conditions is based on physiological data on chemical, physical and hemodynamic heat regulation of tissues and organs of man. Ying *et al.*[1] developed a coupled thermo fluid model to simulate blood flow in large vessels and living tissue. They analyzed the human finger is an extension of the brain and can convey the information on mechanical, thermal and tissue damaging. The quantitative prediction of blood flow rate and heat generation are of great importance for diagnosing blood circulation illness and for the noninvasive measurement of blood glucose. Different physico-mathematical models of SHF hyperthermia was considered by Shul'man[2]. He observed that living bio-tissue have great number of applications in medicine, agriculture, space, aquanautics, military science, everyday life, under tropic and polar conditions, *etc*. Blood flow is an important factor in the formation of temperature fields inside a living body. In local superheating of some object, *e.g.*, a malignant tumor, arterial blood passing through it carries away a portion of heat supplied from without to venous beds and the local temperature of such bio-tissue will be determined mainly by the intensity of the blood flow. Ogulu[3] studied heat and mass transfer flow of blood in a single blood vessel. He modeled blood as a Newtonian fluid of constant properties while the blood vessel is modeled as a long tube of circular section of slowly varying radius. Dynamic response of heat and mass transfer in blood flow through stenosed bifurcated arteries was investigated by Chakravarty and Sen[4]. They observed that the heat and mass transport phenomena of blood always play a key role to the understanding and development of arterial diseases in general and the heat flow together with the transport of macromolecules with dissolved gases to and through the arterial wall influence more on the growth and development of atherogenetic processes, in particular.

The Newtonian and non-Newtonian rheological character of solutions and suspensions with aggregating particles as well as of whole blood and erythrocyte suspensions in isotonic salt solutions is manifested at large concentrations of suspended material[5-10]. Several theoretical and experimental studies have been made to study rheological properties of blood fow are reported[11-15].

Taking into an account the above analysis in mind, we have studied the influence of heat transfer and chemical reactions on Williamson fluid model for blood flow through a tapered artery with a stenosis. To the best of our knowledge no investigation have been made to study the blood flow by treating blood as Williamson fluid. Perturbation solution of the governing equations along with the boundary conditions of stenosed symmetric artery have been calculated. The expressions for velocity, temperature, concentration, resistance impedance,

wall shear stress and shearing stress at the stenosis throat have been examined. The graphical behavior of different type of tapered arteries have been examined for different parameters of interest. Stream lines have been plotted at the end of the article.

Formulation of the problem

Let us consider the flow of an incompressible Williamson fluid lying in a tube having length (L). We are considering cylinderical coordinates system $(\bar{r},\bar{\theta},\bar{z})$ such that $\bar{u}$, $\bar{v}$ and $\bar{w}$ are the velocity components in $\bar{r}$, $\bar{\theta}$ and $\bar{z}$ direction, respectively. Heat and mass transfer phenomena is taken into account by giving temperature $\bar{T}_1$ and concentration $\bar{C}_1$ to the wall of the tube, while at the centre of the tube we are considering symmetry condition on both temperature and concentration. Followed by Mekhiemer *et al.*[11]; the geometry of the stenosis which is assumed to be symmetric is defined as:

$$h(z) = d(z)[1-\eta(b^{n-1}(z-a)-(z-a)^n)], \quad a \le z \le a+b,$$
$$= d(z), \text{otherwise} \tag{1}$$

with

$$d(z) = d_0 + \xi z, \tag{2}$$

where d(z) is the radius of the tapered arterial segment in the stenotic region, d_0 is the radius of the non-tapered artery in the non-stenoic region, ξ is the tapering parameter, b is the length of stenosis, $(n \ge 2)$ is a parameter determining the shape of the constriction profile and referred to as the shape parameter (the symmetric stenosis occurs for n = 2) and a indicates its location as shown in Fig. 1.

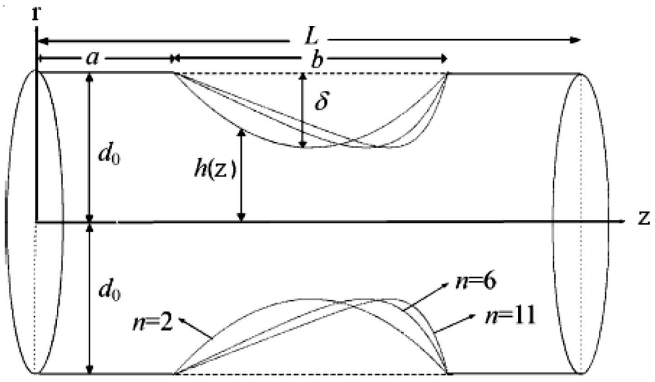

Fig. 1. Geometry of an axially non-symmetrical stenosis in the artery

The parameter η is given by

$$\eta = \frac{\delta^* n^{\frac{n}{n-1}}}{d_0 b^n (n-1)} \tag{3}$$

where δ denotes the maximum height of the stenosis located at

$$z = a + \frac{b}{n^{\frac{n}{n-1}}}$$

The equations which governs the flow are continuity, momentum, energy and mass are

$$\frac{\partial \bar{u}}{\partial \bar{r}} + \frac{\bar{u}}{\bar{r}} + \frac{\partial \bar{w}}{\partial \bar{z}} = 0 \tag{4}$$

$$\rho\left(\bar{u}\frac{\partial}{\partial \bar{r}} + \bar{w}\frac{\partial}{\partial \bar{z}}\right)\bar{u} = -\frac{\partial \bar{p}}{\partial \bar{r}} + \frac{1}{\bar{r}}\frac{\partial}{\partial \bar{r}}(\bar{r}\bar{\tau}_{\bar{r}\bar{z}}) + \frac{\partial}{\partial \bar{z}}(\bar{\tau}_{\bar{r}\bar{z}}) - \frac{\bar{\tau}_{\bar{\theta}\bar{\theta}}}{\bar{r}} \tag{5}$$

$$\rho\left(\bar{u}\frac{\partial}{\partial \bar{r}} + \bar{w}\frac{\partial}{\partial \bar{z}}\right)\bar{w} = -\frac{\partial \bar{p}}{\partial \bar{z}} + \frac{1}{\bar{r}}\frac{\partial}{\partial \bar{r}}(\bar{r}\bar{\tau}_{\bar{r}\bar{z}}) + \frac{\partial}{\partial \bar{z}}(\bar{\tau}_{\bar{z}\bar{z}}) \tag{6}$$

$$\rho c_p\left(\bar{u}\frac{\partial}{\partial \bar{r}} + \bar{w}\frac{\partial}{\partial \bar{z}}\right)\bar{T} = \bar{\tau}_{\bar{r}\bar{r}}\frac{\partial \bar{u}}{\partial \bar{r}} + \bar{\tau}_{\bar{r}\bar{z}}\frac{\partial \bar{w}}{\partial \bar{r}} + \bar{\tau}_{\bar{r}\bar{z}}\frac{\partial \bar{u}}{\partial \bar{z}} + \bar{\tau}_{\bar{z}\bar{z}}\frac{\partial \bar{w}}{\partial \bar{z}} + k\left(\frac{\partial^2 \bar{T}}{\partial \bar{r}^2} + \frac{1}{\bar{r}}\frac{\partial \bar{T}}{\partial \bar{r}} + \frac{\partial^2 \bar{T}}{\partial \bar{z}^2}\right) \tag{7}$$

$$\left(\frac{\partial}{\partial \bar{t}} + \bar{u}\frac{\partial}{\partial \bar{r}} + \bar{w}\frac{\partial}{\partial \bar{z}}\right)\bar{C} = D\left(\frac{\partial^2 \bar{C}}{\partial \bar{r}^2} + \frac{1}{\bar{r}}\frac{\partial \bar{C}}{\partial \bar{r}} + \frac{\partial^2 \bar{C}}{\partial \bar{z}^2}\right) + \frac{DK_T}{T_m}\left(\frac{\partial^2 \bar{T}}{\partial \bar{r}^2} + \frac{1}{\bar{r}}\frac{\partial \bar{T}}{\partial \bar{r}} + \frac{\partial^2 \bar{T}}{\partial \bar{z}^2}\right) \tag{8}$$

In the above equations, $\bar{p}$ is the pressure $\bar{u}$; $\bar{w}$ are the respective velocity components in the radial and axial directions respectively, $\bar{T}$ is the temperature, $\bar{C}$ is the concentration of fluid, ρ is the density, k denotes the thermal conductivity, c_p is the specific heat at constant pressure, T_m is the temperature of the medium, D is the coefficients of mass diffusivity, K_T is the thermal-diffusion ratio.

The constitutive equation for Williamson fluid[15] is defined as

$$S = -PI + \bar{\tau} \tag{9}$$

$$\bar{\tau} = [\eta_\infty + (\eta_0 + \eta_\infty)(1-\Gamma\bar{\dot{\gamma}})^{-1}]\bar{\dot{\gamma}} \tag{10}$$

in which -PI is the spherical part of the stress due to constraint of incompressibility, $\bar{\tau}$ is the extra stress tensor, η_∞ is the infinite shear rate viscosity, η_0 is the zero shear rate viscosity, Γ is the time constant and $\bar{\dot{\gamma}}$ is defined as

$$\bar{\dot{\gamma}} = \sqrt{\frac{1}{2}\sum_i\sum_j \bar{\dot{\gamma}}_{ij}\bar{\dot{\gamma}}_{ji}} = \sqrt{\frac{1}{2}\Pi} \tag{11}$$

Here Π is the second invariant strain tensor. We consider the constitutive eqn. 7, the case for which $\eta_\infty = 0$ (because we cannot find the solution at the infinite shear rate viscosity).

The component of extra stress tensor therefore, can be written as

$$\bar{\tau} = \eta_0[(1-\Gamma\bar{\dot{\gamma}})^{-1}]\bar{\dot{\gamma}} = \eta_0[(1+\Gamma\bar{\dot{\gamma}})]\bar{\dot{\gamma}} \tag{12}$$

We introduce the non-dimensional variables

$$r = \frac{\bar{r}}{d_0}, z = \frac{\bar{z}}{b}, w = \frac{\bar{w}}{u_0}, u = \frac{b\bar{u}}{u_0\delta}, p = \frac{d_0^2\bar{p}}{u_0 b\eta_0}, h = \frac{\bar{h}}{d_0}$$

$$Re = \frac{\rho b u_0}{\eta_0}, \bar{\tau}_{rr} = \frac{b\bar{\tau}_{rr}}{u_0\eta_0}, \bar{\tau}_{rz} = \frac{d_0\bar{\tau}_{rz}}{u_0\eta_0}, \bar{\tau}_{zz} = \frac{b\bar{\tau}_{zz}}{u_0\eta_0}, \bar{\tau}_{\theta\theta} = \frac{b\bar{\tau}_{\theta\theta}}{u_0\eta_0}$$

$$We = \frac{\Gamma u_0}{d_0}, \theta = \frac{\bar{T}-\bar{T}_1}{\bar{T}_0-\bar{T}_1}, E_c = \frac{u_0^2}{c_p(\bar{T}_0-\bar{T}_1)}, Pr = \frac{c_p\eta_0}{k}$$

$$Sr = \frac{\rho DK_T(\bar{T}_0-\bar{T}_1)}{\eta_0 T_m(\bar{C}_0-\bar{C}_1)}, S_c = \frac{\eta_0}{D\rho}, \sigma = \frac{(\bar{C}-\bar{C}_1)}{(\bar{C}_0-\bar{C}_1)} \tag{13}$$

in which S_r is the Soret number, S_c Schmidt number, u_0 is the velocity averaged over the section of the tube of the width d_0 and σ is concentration.

Making use of eqns. 12 and 13; into eqns. 4 to 8, the appropriate equations describing the steady flow of an incompressible Williamson fluid in the case of mild stenosis $\left(\frac{\delta^*}{d_0} << 1\right)$, subject to the additional conditions[11]

$$(i)\frac{Re\,\delta^* n^{\left(\frac{1}{n-1}\right)}}{b} << 1 \tag{14a}$$

$$(ii)\frac{d_0 n^{\left(\frac{1}{n-1}\right)}}{b} \sim O(1) \tag{14b}$$

can be written as

$$\frac{\partial u}{\partial r}+\frac{u}{r}+\frac{\partial w}{\partial z}=0 \tag{15}$$

$$\frac{\partial p}{\partial r}=0 \tag{16}$$

$$\frac{\partial p}{\partial z}=\frac{1}{r}\frac{\partial}{\partial r}\left\{r\left[\left(\frac{\partial w}{\partial r}\right)+We\left(\frac{\partial w}{\partial r}\right)^2\right]\right\} \tag{17}$$

$$\frac{1}{r}\frac{\partial}{\partial r}\left(r\frac{\partial \theta}{\partial r}\right)+B_r\left\{\left(\frac{\partial w}{\partial r}\right)^2+We\left(\frac{\partial w}{\partial r}\right)^3\right\}=0 \tag{18}$$

$$\frac{1}{S_c}\left\{\frac{1}{r}\frac{\partial}{\partial r}\left(r\frac{\partial \sigma}{\partial r}\right)\right\}+S_r\left\{\frac{1}{r}\frac{\partial}{\partial r}\left(r\frac{\partial \theta}{\partial r}\right)\right\}=0 \tag{19}$$

where $B_r = E_c\,Pr$.

The imposed boundary conditions for the problem under consideration are

$$\frac{\partial w}{\partial r}=0,\frac{\partial \theta}{\partial r}=0,\frac{\partial \sigma}{\partial r}=0 \text{ at } r=0 \tag{19a}$$

$$w=0,\ \theta=0,\ \sigma=0 \text{ at } r=h(z) \tag{19b}$$

where

$$h(z)=(1+\xi z)[1-\eta_1((z-\sigma)-(z-\sigma)^n)]$$

$$\sigma \le z \le \sigma+1$$

and

$$\eta_1=\frac{\delta n^{\frac{n}{n-1}}}{(1-1)},\delta=\frac{\delta^*}{d_0},\sigma=\frac{a}{b},\xi'=\frac{\xi b}{d_0}$$

where $\xi = \tan\phi$, ϕ is called tappered angle and for converging tapering ($\phi < 0$), non-tapered artery ($\phi = 0$) and the diverging tapering ($\phi > 0$) (as shown in Fig. 2).

Solution of the problem

Perturbation solution: To get the perturbation solution we expand w, θ, p and Q by taking We as a perturbation parameter as follow

$$w = w_0 + We\ w_1 + O\ (We)^2 \tag{20a}$$

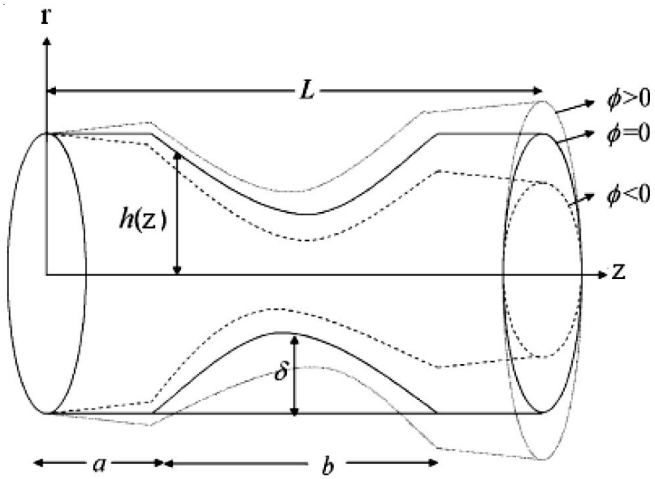

Fig. 2. Geometry of the axially stenosied tapered artery for different tapered angle

$$\theta = \theta_0 + We\ \theta_1 + O\ (We)^2 \tag{20b}$$

$$p = p_0 + We\ p_1 + O\ (We)^2 \tag{20c}$$

$$Q = Q_0 + We\ Q_1 + O\ (We)^2 \tag{20d}$$

Expression for velocity, temperature, concentration field and pressure gradient for small We can be written as follows

$$w(r,z)=\frac{dp}{dz}\left(\frac{r^2-h^2}{4}\right)-We\left(\frac{64Q^2(r^3-h^3)}{3h^8}\right) \tag{21}$$

$$\theta(r,z)=-B_r\left\{\left(-\frac{16Q}{h^4}\right)^2\left(\frac{r^4-h^4}{64}\right)+We\left[\left(\frac{dp_1}{dz}\right)^2\left(\frac{r^4-h^4}{64}\right)+\left(-\frac{16Q}{h^4}\right)^4\left(\frac{r^6-h^6}{576}\right)-\left(\frac{dp_1}{dz}\right)\left(-\frac{16Q}{h^4}\right)^2\left(\frac{r^5-h^5}{100}\right)+\left(-\frac{16Q}{h^4}\right)^3\left(\frac{r^5-h^5}{100}\right)\right]\right\} \tag{22}$$

$$\sigma(r,z)=S_rS_cB_r\left\{\left(-\frac{16Q}{h^4}\right)^2\left(\frac{r^4-h^4}{64}\right)+We\left[\left(\frac{dp_1}{dz}\right)^2\left(\frac{r^4-h^4}{64}\right)+\left(-\frac{16Q}{h^4}\right)^4\left(\frac{r^6-h^6}{576}\right)-\left(\frac{dp_1}{dz}\right)\left(-\frac{16Q}{h^4}\right)^2\left(\frac{r^5-h^5}{100}\right)+\left(-\frac{16Q}{h^4}\right)^3\left(\frac{r^5-h^5}{100}\right)\right]\right\} \tag{23}$$

$$\frac{dp}{dz}=-\frac{16Q}{h^4}+We\left(\frac{512Q^2}{5h^7}\right) \tag{24}$$

The pressure drop ($\Delta p = p$ at $z = 0$ and $\Delta p = -p$ at $z = L$) across the stenosis between the section $z = 0$ and $z = L$ is obtain from (24) as done by [5] is de.ned as

$$\Delta p=\int_0^L\left(-\frac{dp}{dz}\right)dz \tag{25}$$

Resistance impedance

The expression for resistance impedance is obtained from eqn. 25 defined as:

$$\tilde{\lambda} = \frac{\Delta p}{Q} = 4\left\{\int_0^a F(z)\,|_{h=1}\,dz + \int_a^{a+b} F(z)dz + \int_{a+b}^{L} F(z)\,|_{h=1}\,dz\right\} \quad (26)$$

where

$$F(z) = \frac{4}{h^4} - We\left(\frac{128Q}{5h^7}\right) \quad (27)$$

Eqn. 26 can also be written as

$$\tilde{\lambda} = 4\left\{(L-b)\left(4 - We\left(\frac{128Q}{5}\right)\right) + \int_a^{a+b} F(z)dz\right\} \quad (28)$$

Expression for the wall shear stress

The expression for wall shear stress is defined as

$$\tilde{\tau}_{rz} = \left\{\left(\frac{\partial w}{\partial r}\right) + We\left(\frac{\partial w}{\partial r}\right)^2\right\}\Bigg|_{r=h} \quad (29)$$

With the help of eqn. 21; eqn. 29 takes the following form

$$\tilde{\tau}_{rz} = [4QR(z) + 16WeQ^2(R(z))^2] \quad (30)$$

where

$$R(z) = \frac{F(z)h}{2} - \frac{16WeQ}{h^6} \quad (31)$$

The shearing stress at the stenosis throat located at z = $\frac{a}{b} + \frac{1}{n^{\frac{n}{n-1}}}$ *i.e.*, $\tilde{\tau}_s = \tilde{\tau}_{rz}\,|_{h=1-\delta}$

$$\tilde{\tau}_s = [4QJ + 16WeQ^2(J)^2] \quad (32)$$

where

$$J = \frac{K(1-\delta)}{2} - \frac{16WeQ}{(1-\delta)^6}$$

$$K = \frac{4}{(1-\delta)^4} + We\left(\frac{128Q}{5(1-\delta)^7}\right) \quad (33)$$

The final expressions for the dimensionless resistance to λ, wall shear stress τ_{rz} and the shearing stress at the throat τ_s are defined as follows

$$\lambda = \frac{4}{3}\left\{\left(1 - \frac{b}{L}\right)\left(4 - We\left(\frac{128Q}{5}\right)\right) + \frac{1}{L}\int_a^{a+b} F(z)dz\right\} \quad (34)$$

$$S_{rz} = [R(z) + 4WeQ(R(z))^2] \quad (35)$$

$$\tau_s = [J + 4WeQ(J)^2] \quad (36)$$

in which

$$\lambda = \frac{\tilde{\lambda}}{\lambda_0}, \tau_{rz} = \frac{\tilde{\tau}_{rz}}{\tau_0}, \tau_s = \frac{\tilde{\tau}_s}{\tau_0}, \lambda_0 = 3L, \tau_0 = 4Q$$

here λ_0, τ_0 are the resistance to flow and the wall shear stress for a flow in a normal artery (no stenosis).

RESULTS AND DISCUSSION

The quantitative effects of the Weissenberg number (We); the stenosis shape n and maximum height of the stenosis δ for converging tapering, diverging tapering and non-tapered arteries for Williamson fluid are observed physically through Figs. 3-15. Figs. 3-6 are prepared to see the variation of impedance resistance for different parameters of interest, it is noticed that the impedance resistance decreases for converging tapering, diverging tapering and non-tapered arteries when we increase n, L, We and Q. We also observed that resistive impedance in a diverging tapering appear to be smaller than those in converging tapering because the flow rate is higher in the former than that in the latter, as anticipated and impedance resistance attains its maximum values in the symmetric stenosis case (n = 2). Figs. 7-9 show, how the converging tapering, diverging tapering and non-tapered arteries influence on the wall shear stress τ_{rz}. It is observed that with an increase in n, δ and We shear stress increases, the stress yield diverging tapering with tapered angle $\phi > 0$, converging tapering with tapered angle $\phi < 0$ and non-tapered artery with tapered angle $\phi = 0$. Figs. 10 and 11 are prepared to see the variation of the shearing stress at the stenosis throat τ_s with δ. It is analyzed through figures that shearing stress at the stenosis throat increases with an increase in Q and decreases with an increase in We. It is also depicted that shearing stress at the throat τ_s possess an inverse variation to the flow resistance λ with respect to flow rate Q and Weissenberg number (We). Finally, the variation of axial velocity for m, We, δ and n for the case of a converging tapering, diverging tapering and non-tapered arteries are displayed in Figs. 12-15. From Figs. 12-15, we observed that with an increase in We, δ and n velocity profile decreases while increases with an increase in Q. It is also seen that for the case of converging tapering velocity gives larger values as compared to the case of diverging tapering and non-tapered arteries. Figs. 16 and 17 show the variation of temperature profile for different values of Brickmann number B_r and Weissenberg number We. It is observed that with an increase in Brickmann number B_r and Weissenberg number (We), temperature profile increases and temperature profile gives the large values for converging tapering as compared to the diverging and non-tapered artery. Figs. 18 and 19 are prepared to see the variation of concentration profile for Brickmann number B_r and Soret number S_r. It is observed that with an increase in Brickmann number B_r and Soret number S_r, concentration profile decreases. It is also seen that concentration profile has an opposite behaviour as compared to the temperature profile. Trapping phenomena have been discussed through Figs. 20-23. Fig. 20 shows the stream lines for different values of tappered angle ϕ. It is observed that size of trapping bolus is small for diverging tapering as compared to the converging tapering and non-tapered arteries. Stream lines for different values of the stenosis shape n is prepared in Fig. 21. It is analyzed that the size of the trapping bolus decreases when we increase the stenosis shape. Figs. 22 and 23 are plotted to see the stream lines for different values of height of the stenosis δ and Weissenberg number (We). It is depicted that the size of the trapping bolus decreases with an increase in the height of the stenosis and Weissenberg number.

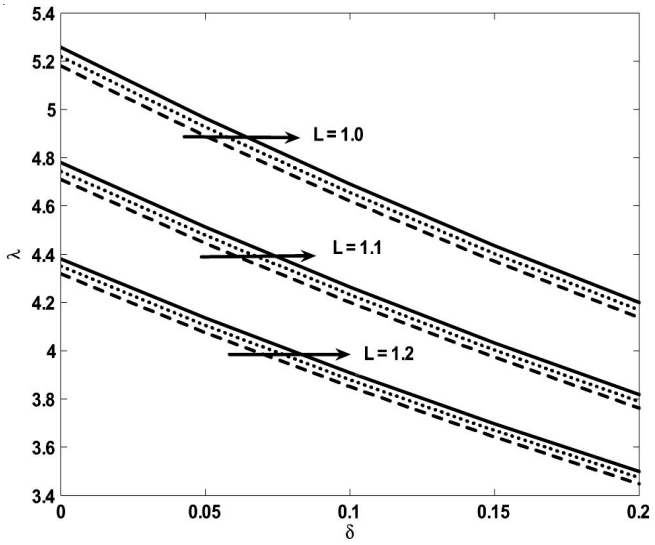

Fig. 3. Variation of resistance for Q = 0.2, We = 0.1, b = 1, σ = 0.0; n = 2, z = 0.5

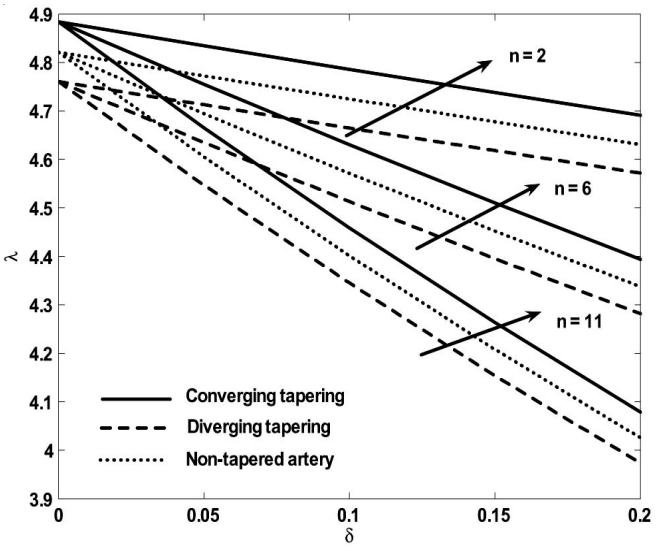

Fig. 4. Variation of resistance for Q = 0.9, We = 0.1; b = 1, σ = 0.0, L = 1, z = 0.95

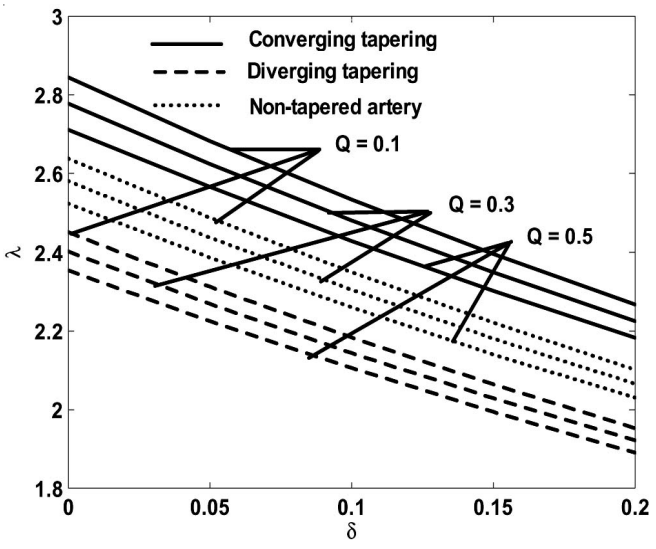

Fig. 5. Variation of resistance for n = 2, We = 0.1; b = 1, σ = 0.0; L = 2, z = 0.95

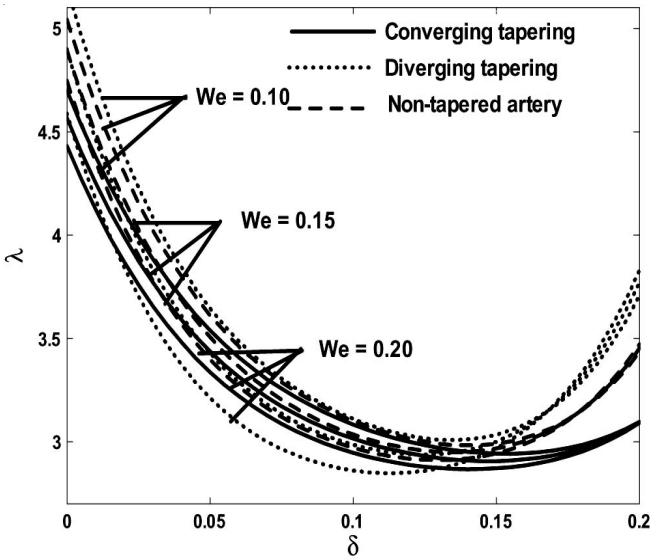

Fig. 6. Variation of resistance for n = 2, Q = 0.1, b = 1, σ = 0.0, L = 2, z = 0.95

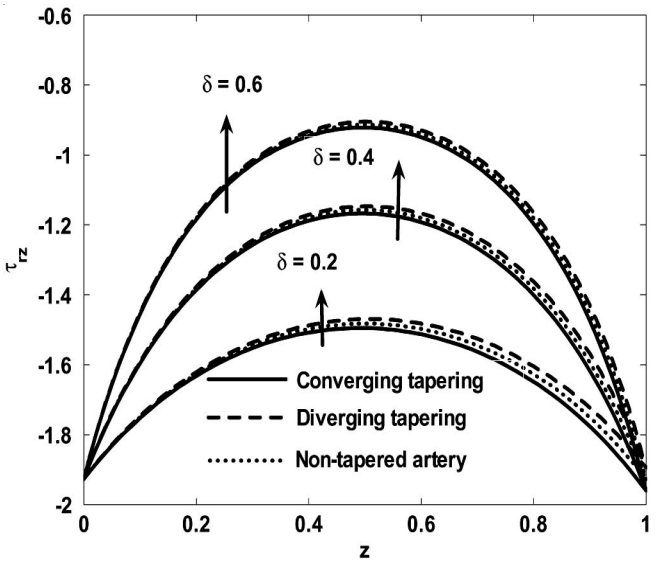

Fig. 7. Variation of wall stress for Q = 0.02, We = 0.5, σ = 0.0; n = 2

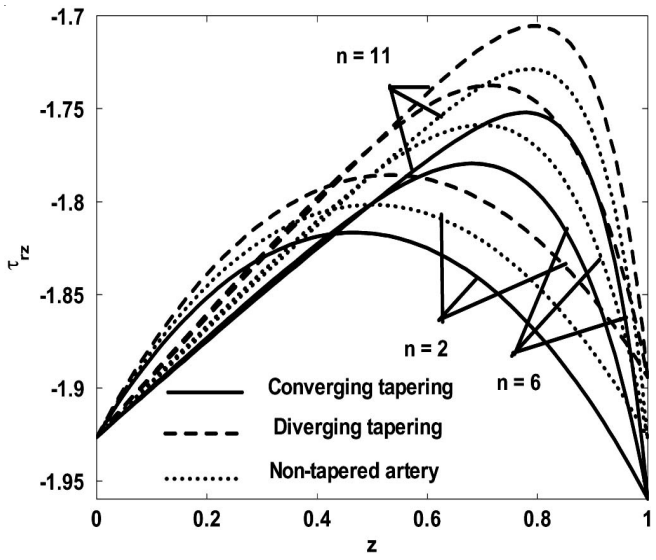

Fig. 8. Variation of wall stress for Q = 0.02, We = 0.5, σ = 0.0, δ = 0.05

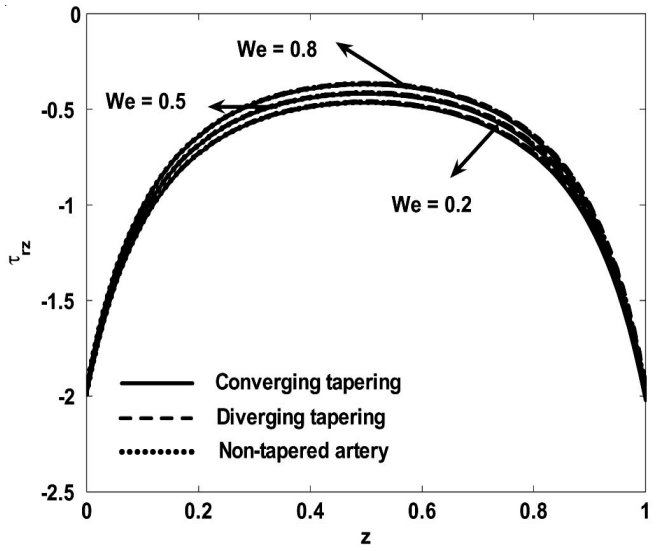

Fig. 9. Variation of wall stress for Q = 0.02, n = 2, σ = 0.0, δ = 1.5

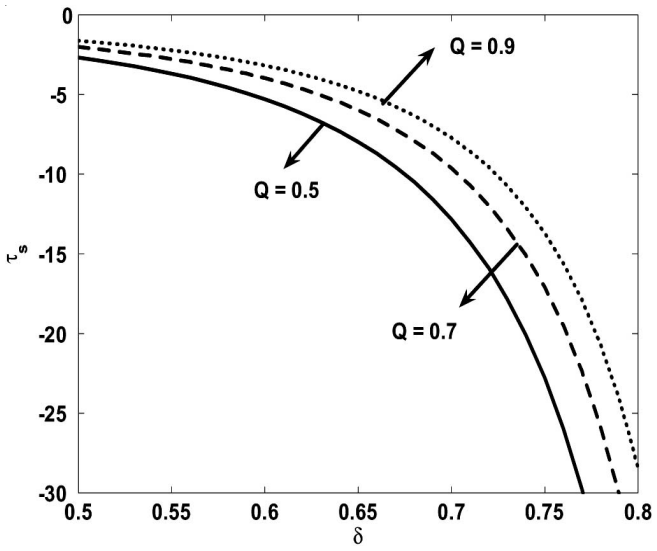

Fig. 10. Variation of shear stress at the stenosis throat for We = 0.5

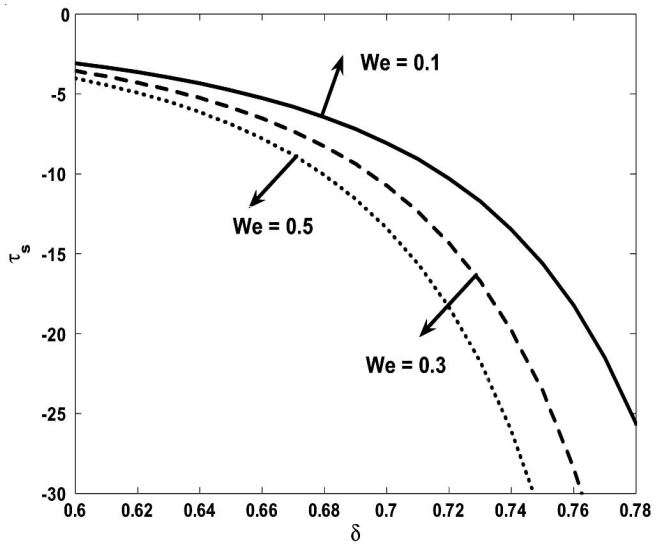

Fig. 11. Variation of shear stress at the stenosis throat for Q = 0.8

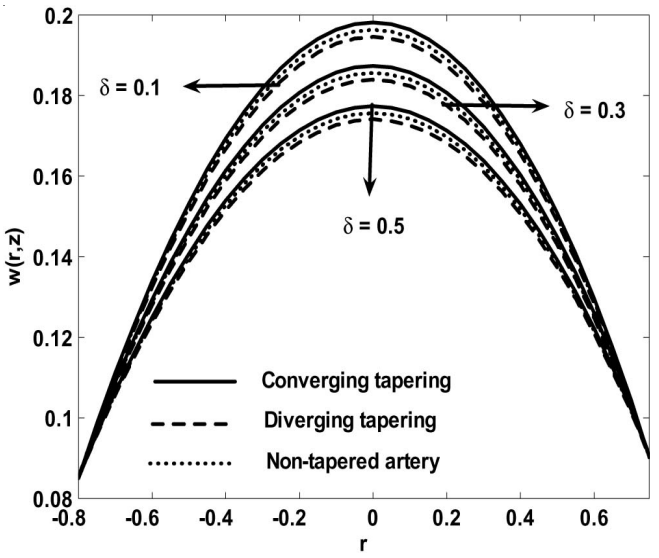

Fig. 12. Variation of velocity profile for Q = 0.05, We = 0.2, n = 2, z = 0.95, σ = 0.00

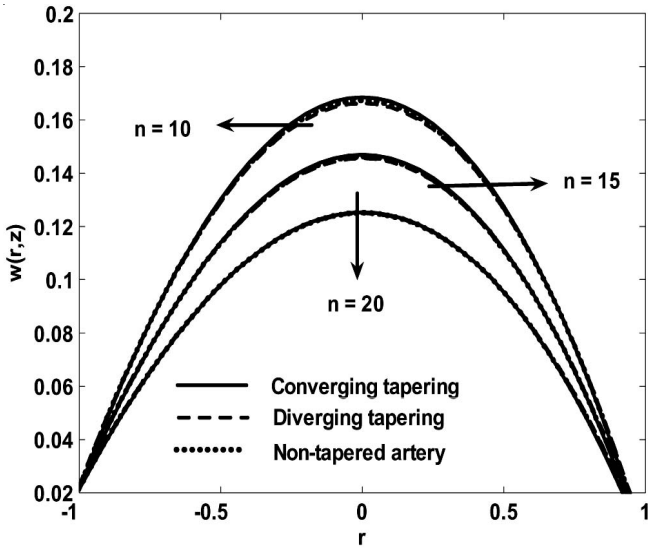

Fig. 13. Variation of velocity profile for Q = 0.02, We = 0.2, δ = 0.005, z = 0.9, σ = 0.00

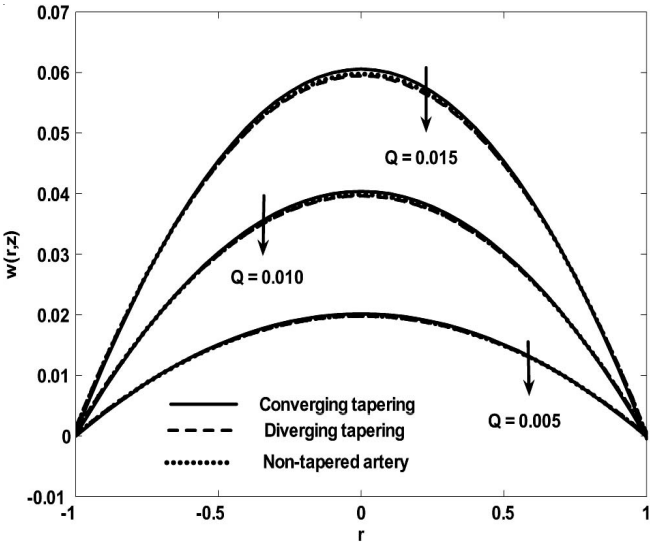

Fig. 14. Variation of velocity profile for n = 2, We = 0.1, δ = 0.005, z = 0.9, σ = 0.00

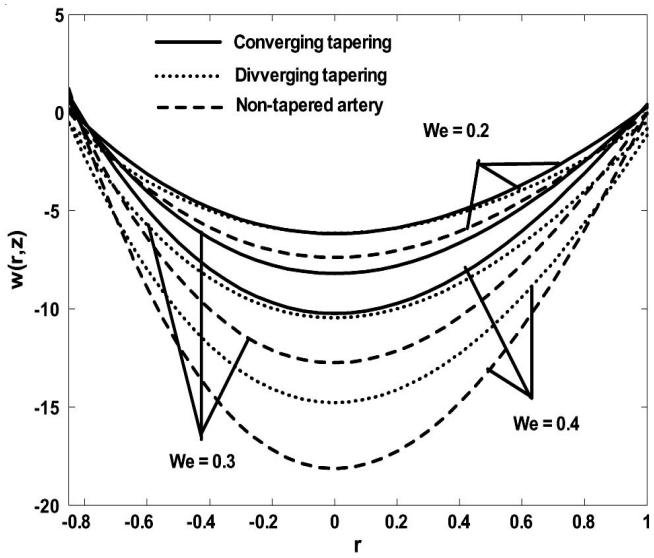

Fig. 15. Variation of velocity profile for n = 2, Q = 0.8, δ = 0.005, z = 0.09, σ = 0.00

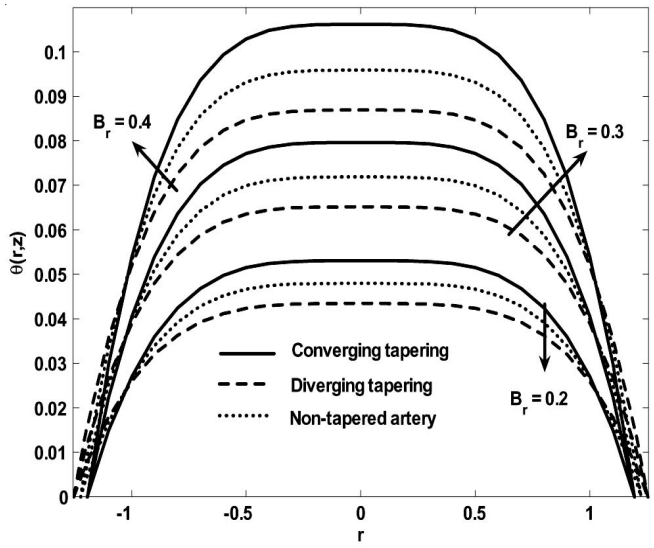

Fig. 16. Variation of temperature profile for n = 11, Q = 0.3, δ = 0.5, z = 0.5, σ = 0.00, We = 0.5

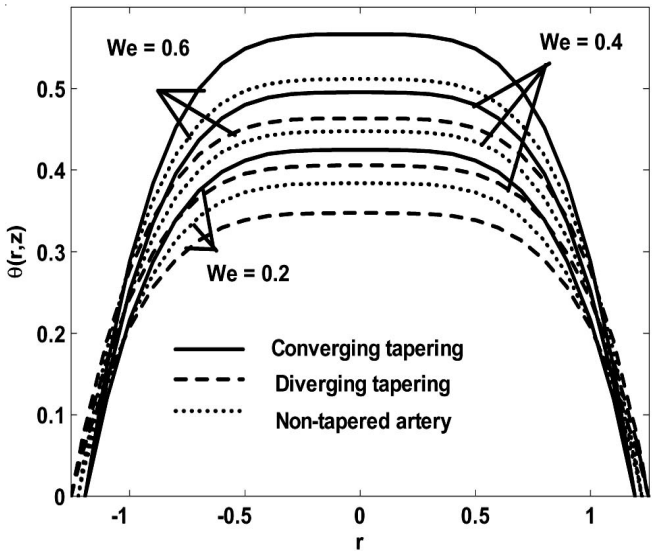

Fig. 17. Variation of temperature profile for n = 11, Q = 0.3, δ = 0.5, z = 0.5, σ = 0.00; B_r = 2

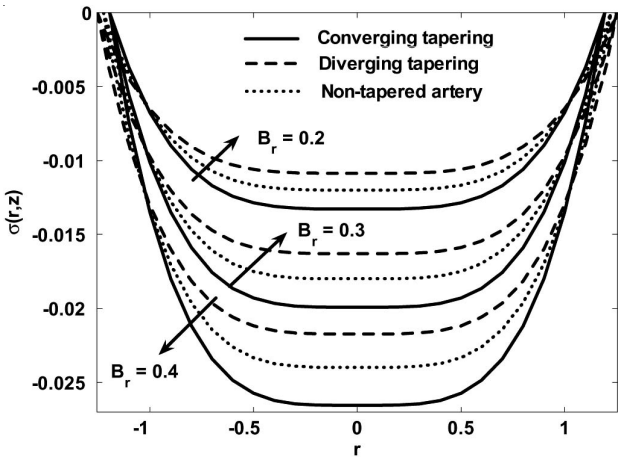

Fig. 18. Variation of concentration profile for n = 11, Q = 0.3, δ = 0.5, z = 0.5, σ = 0.00, We = 0.5, S_r = 0.5, S_c = 0.5

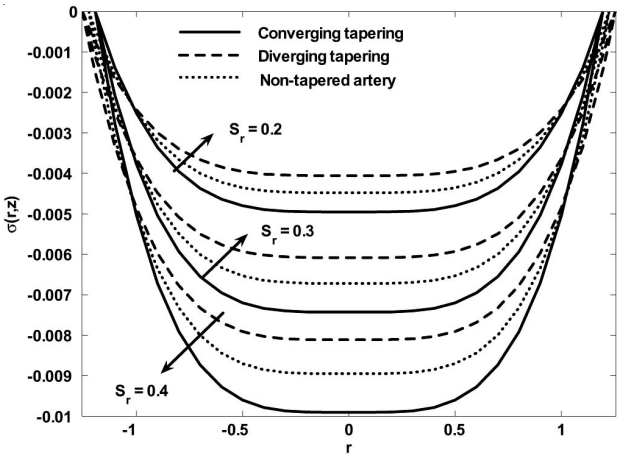

Fig. 19. Variation of concentration profile for n = 11, Q = 0.3, δ = 0.5, z = 0.5, σ = 0.00, We = 0.5, B_r = 2, S_c = 0.5

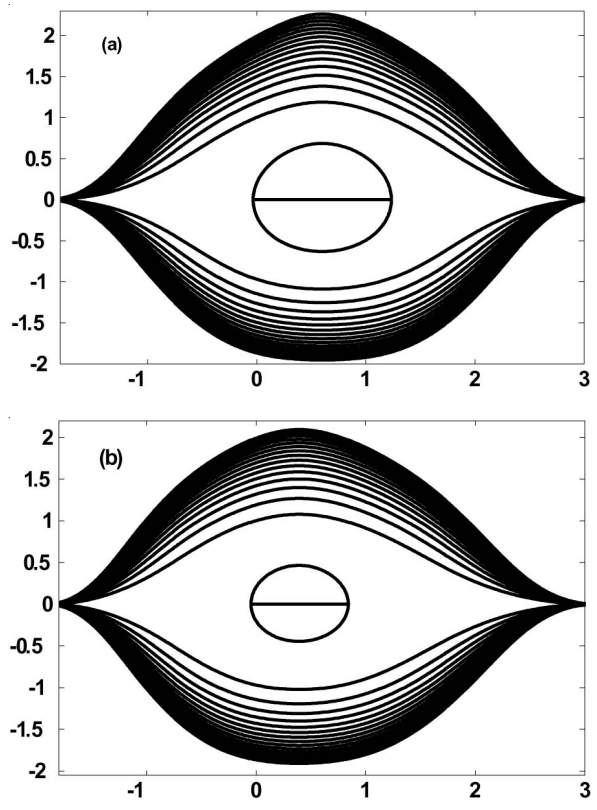

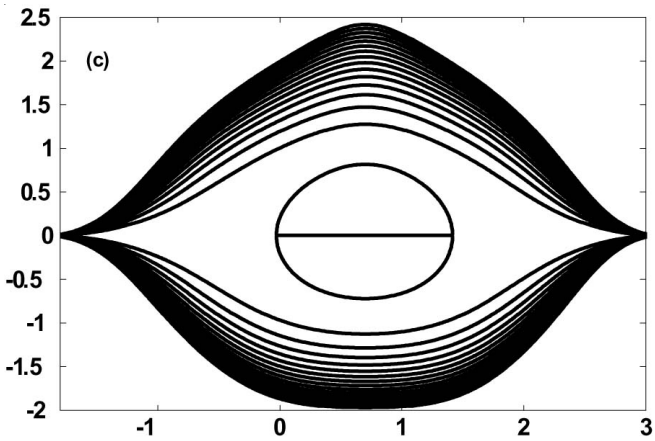

Fig. 20. Stream lines for different values of tapered angles (a) Converging tapering (b) Diverging tapering (c) Non-tapered artery for n = 2, Q = -0.1, $\delta = 0.1$, $\sigma = 0.1$, $W_e = 0.2$

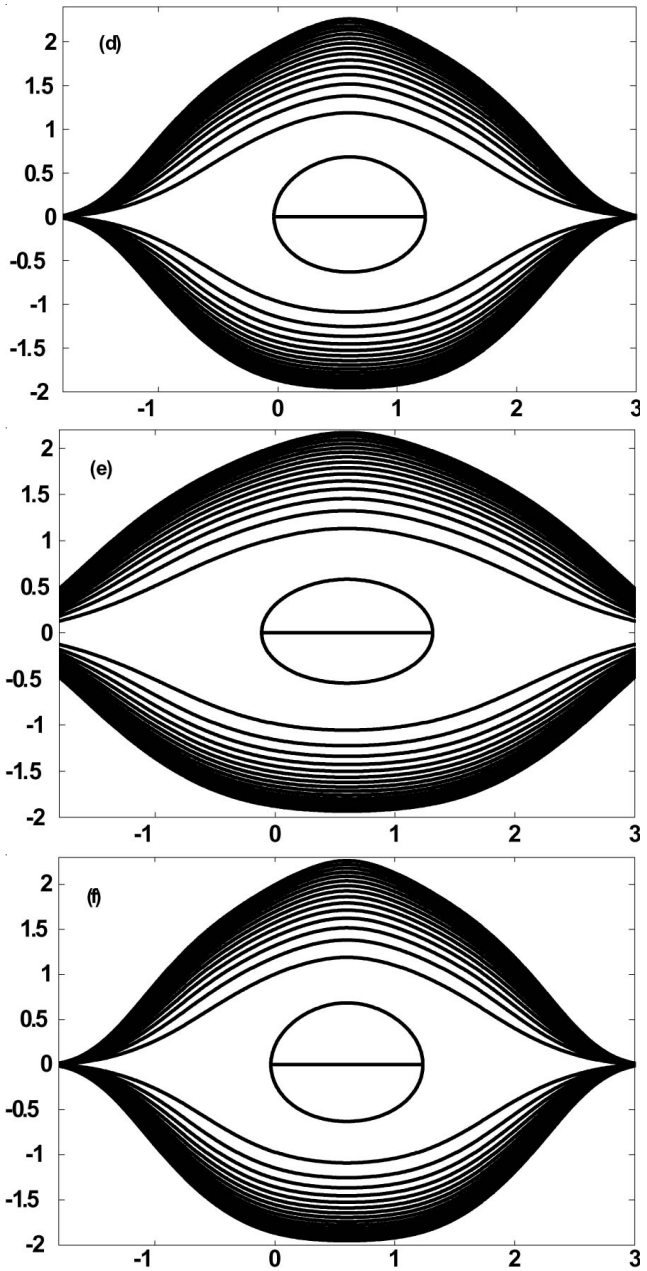

Fig. 21. Stream lines for different values of n (d) n = 2 (e) n = 4 (f) n = 6 for $\phi = 3.147$, Q = -0.1, $\delta = 0.1$, $\sigma = 0.1$, We = 0.2

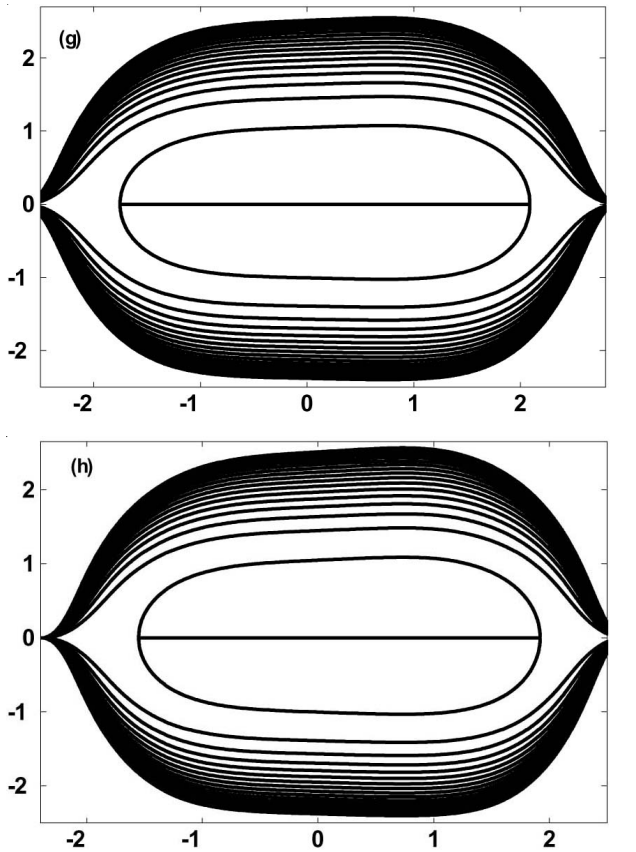

Fig. 22. Stream lines for different values of δ (g) $\delta = 0.1$ (h) $\delta = 0.2$ for $\phi = 3.147$, Q = -0.1, n = 2, $\sigma = 0.1$, We = 0.2

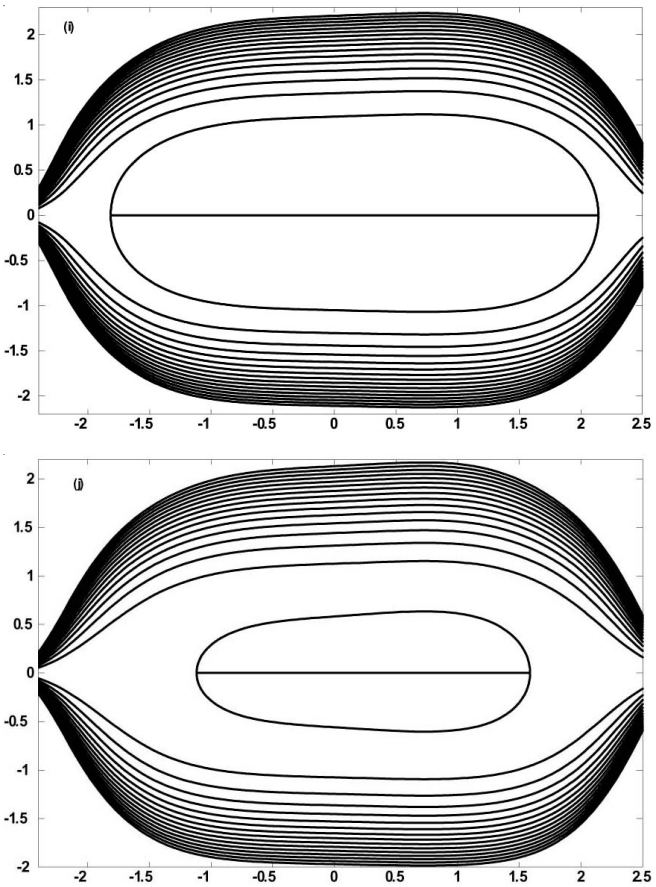

Fig. 23. Stream lines for different values of We (i) We = 0.1 (j) We = 0.2 for $\phi = 3.147$, Q = - 0.1, n = 2, $\sigma = 0.1$, $\delta = 0.2$

ACKNOWLEDGEMENTS

This research was supported by the WCU (World Class University) program and the ERC program through the National Research Foundation of Korea (NRF) funded by the Ministry of Education, Science and Technology (R31-2008-000-10049-0 and 20090093134).

REFERENCES

1. Y. He, H. Liu, R. Himeno, J. Sunaga, N. Kakusho and H. Yokota, *Comp. Biol. Med.*, **38**, 555 (2008).
2. Z.P. Shulman, *J. Eng. Phys. Thermophys.*, **69**, 356 (1996).
3. A. Ogulu, *Int. Commun. Heat Mass Trans.*, **33**, 790 (2006).
4. S. Chakravarty and S. Sen, *Korea-Australia Rheol. J.*, **17**, 47 (2005).
5. S. Nadeem, T. Hayat, N.S. Akbar and M.Y. Malik, *Int. J. Heat Mass Trans.*, **52**, 4722 (2009).
6. S. Nadeem and N.S. Akbar, *Commun. Non-linear Sci. Numer. Simulat.*, **14**, 4100 (2009).
7. M. Kothandapani and S. Srinivas, *Int. J. Non-linear Mechan.*, **43**, 915 (2008).
8. M. Kothandapani and S. Srinivas, *Phys. Lett A*, **372**, 4586 (2008).
9. S. Srinivas and R. Gayathri, *Appl. Math. Comput.*, **215**, 185 (2009).
10. S. Srinivas, R. Gayathri and M. Kothandapani, *Comp. Phys. Commun.*, **180**, 2115 (2009).
11. Kh.S. Mekheimer and M.A. El Kot, *Acta Mech. Sin.*, **24**, 637 (2008).
12. Kh.S. Mekheimer and M.A. El Kot, *Appl. Math. Mech.*, **29**, 1093 (2008).
13. Kh.S. Mekheimer, *Phys. Lett. A*, **372**, 4271 (2008).
14. Kh.S. Mekheimer, *Appl. Math. Comput.*, **153**, 763 (2004).
15. S. Nadeem and N.S. Akbar, *Int. J. Numer. Methods for fluids*, **66**, 919 (2011).